European Journal of Chemistry

View Journal Online
View Article Online

Synthesis, spectral, crystallographic, and computational investigation of a novel molecular hybrid 3-(1-((benzoyloxy)imino)ethyl)-2*H*-chromen-2-ones

Kannan Gokula Krishnan [1,2] and Venugopal Thanikachalam [2,*]

[1] *Department of Chemistry, Government Arts and Science College for Women, Karimangalam - 635 111, Tamil Nadu, India*
gokulakrishnank83@gmail.com (K.G.K.)
[2] *Department of Chemistry, Annamalai University, Annamalainagar - 608 002, Tamil Nadu, India*
profvt.chemau@gmail.com (V.T.)

* *Corresponding author at: Department of Chemistry, Annamalai University, Annamalainagar - 608 002, Tamil Nadu, India.*
e-mail: profvt.chemau@gmail.com (V. Thanikachalam).

RESEARCH ARTICLE

10.5155/eurjchem.12.2.133-146.2073

Received: 21 January 2021
Received in revised form: 28 February 2021
Accepted: 07 March 2021
Published online: 30 June 2021
Printed: 30 June 2021

KEYWORDS

NMR
Oxime esters
NBO analysis
Single crystal XRD
Vibrational frequencies
Computational chemistry

ABSTRACT

Synthesis of 3-(1-((benzoyloxy)imino)ethyl)-2*H*-chromen-2-ones (1-5) was accomplished and it was characterized experimentally using various analytical techniques. Computational studies have been carried out for all compounds 1-5 using B3LYP method with 6-311++G(d,p) basis set. The optimized structural features *viz*. bond lengths, bond angles, and dihedral angles are compared with their single-crystal X-ray diffraction results of compound 1 (Crystal data for $C_{18}H_{13}NO_4$ (M = 307.29 g/mol): Monoclinic, space group $P2_1/c$ (no. 14), a = 11.399(5) Å, b = 5.876(5) Å, c = 21.859(5) Å, β = 91.060(5)°, V = 1463.9(14) Å^3, Z = 4, T = 293(2) K, μ(MoKα) = 0.100 mm^{-1}, *Dcalc* = 1.394 g/cm^3, 13555 reflections measured (3.58° ≤ 2Θ ≤ 56.98°), 3669 unique (R_{int} = 0.0235) which were used in all calculations. The final R_1 was 0.0444 (>2sigma(I)) and wR_2 was 0.1506 (all data)), which are in good conformity with each other. Normal modes of vibrational frequencies of compounds 1-5 acquired from density-functional theory (DFT) method coincided with the experimental ones. The ^{1}H and ^{13}C chemical shifts of compounds 1-5 have been calculated by GIAO method and the results have been compared with the experimental ones. The first-order hyperpolarizability and their related properties of the novel molecules 1-5 are calculated computationally. The other parameters like natural bond orbital, zero-point vibrational energy, E_{HOMO}, E_{LUMO}, heat capacity and entropy have also been discussed.

Cite this: *Eur. J. Chem.* **2021**, *12(2)*, 133-146 **Journal website**: www.eurjchem.com

1. Introduction

Oxygen containing heterocycles are ubiquitous in a broad spectrum of organic molecules and they are essential in synthetic organic chemistry and drug discovery [1]. Coumarin and its derivatives have been extensively studied due to their excellent pharmacological activity and its wide occurrence in various species of plants. Particularly, plants belonging to the natural orders of orchids (*orchidaceae*), legumes (*leguminosae*), tonkabeans (*dipteryxodorata*), apiaceae (*umbelliferae*), labiatae and rutaceae are rich sources of naturally occurring coumarins [2].

Coumarins have been assorted with therapeutic findings which include antimicrobial, anti-cancer, anticoagulant, antiviral, anti-inflammatory, and antioxidant properties [3-9]. Besides the potential medicinal applications, coumarin has also been used in chemosensors, dye sensitizers, photo triggers, fluorescent labels and probes in biology and medicine [10-13]. Lately, derivatives of coumarin like 3-acyl, 3-benzoyl and 3-carboxamido-2*H*-chromen-2-ones have a keen to significant role in the treatment of neuropsychiatric disorders [14,15].

Oximes [16] and their derivatives like ethers, esters, and carbonates have been privileged over the past decades because of their wide range of pharmaceutical activities and biological functions. Especially, oxime esters have established a biologically active molecule which includes anti-microbial, anti-convulsant, RBBP9, larvicidal activities, and agrochemical industries [17-21]. Recently, oxime esters have been reported to exhibit DNA-cleaving [22] ability in a process that is triggered by UV light.

The structural diversity of organic molecules owing to coumarin moieties reported in the literature stimulated us to proceed with the research on oxime ester moieties and we herein report the synthesis and computational investigation on compounds **1**-**5**. The molecular structural parameters, vibrational frequencies, and nuclear resonance spectra have been computed for the synthesized compounds **1**-**5** with B3LYP/6-311++G(d,p) level of calculations. Theoretical results like optimized structural features, FT-IR, FT-Raman assignment, ^{1}H and ^{13}C chemical shift values are compared with the experimental ones which are in good agreement with each other. HOMO-LUMO energy, Natural Bond Orbital (NBO) analysis, Non-Linear Optical (NLO), and thermodynamic properties were also discussed.

ISSN 2153-2249 (Print) / ISSN 2153-2257 (Online)
https://dx.doi.org/10.5155/eurjchem.12.2.133-146.2073

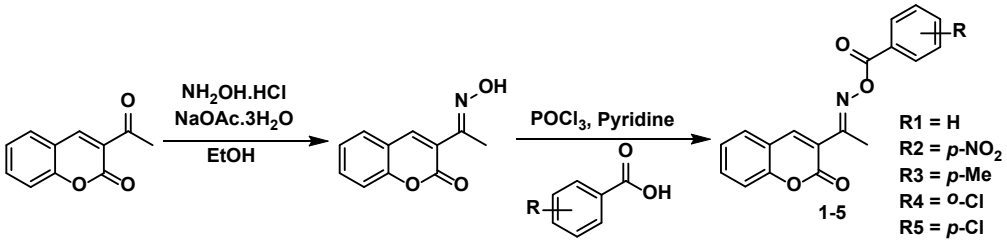

Scheme 1. Synthesis of 3-(1-((benzoyloxy)imino)ethyl)-2*H*-chromen-2-ones (**1-5**).

2. Experimental

2.1. General procedure for the synthesis of 3-(1-((benzoyloxy)imino)ethyl)-2H-chromen-2-ones (1-5)

To a stirred solution of benzoic acid (0.335 g, 2.75 mmol) in dry pyridine (5 mL), $POCl_3$ (0.25 mL, 2.75 mmol) was added drop wise. After 5 min, 3-(1-(hydroxyimino)ethyl)-2*H*-chromen-2-one (0.5 g, 2.5 mmol) was added to the reaction mixture, stirring was continued for 20 min and the progress of the reaction was monitored by TLC. Upon completion of the reaction, a saturated solution of $NaHCO_3$ was added portion wise to the reaction mixture and the crude product was thrown out as a precipitate and the precipitate was filtered, then recrystallized from ethanol to get the pure 3-(1-((benzoyloxy)imino)ethyl)-2*H*-chromen-2-one **1** with an excellent yield (0.65 g, 84%). The above general method was adopted for the synthesis of compounds **2-5** (Scheme 1). The melting points of compounds **1-5** were measured in open capillaries and are uncorrected.

3-(1-((Benzoyloxy)imino)ethyl)-2H-chromen-2-one (**1**): Color: Colorless solid. Yield: 84%. M.p.: 138-140 °C. FT-IR (KBr, ν, cm^{-1}): 2849-3090 (C-H str.), 1739 (C=$O_{lactone}$ str.), 1694 (C=O_{ester} str.), 1622 (C=N str.), 1604 (C=C str.), 701 (N-O str.). ^{1}H NMR (400 MHz, $CDCl_3$, δ, ppm): 8.21 (s, 1H, Ar-H), 8.10 (t, 2H, Ar-H), 7.33-7.64 (m, 7H, Ar-H), 2.56 (s, 3H, CH_3). ^{13}C NMR (100 MHz, $CDCl_3$, δ, ppm): 16.09 (CH_3), 163.66 (C=O_{ester}), 159.29 (C=$O_{lactone}$), 154.39 (C=N), 162.74, 143.60, 133.75, 133.70, 133.47, 133.05, 130.61, 130.20, 129.79, 129.66, 129.35, 129.16, 128.92, 128.73, 128.66, 128.51, 125.00, 123.47, 118.55, 116.72 (aromatic carbons). Anal. calcd. for for $C_{18}H_{13}NO_4$: C, 70.35; H, 4.26; N, 4.56. Found: C, 70.32; H, 4.28; N, 4.55%.

3-(1-(((4-Nitrobenzoyl)oxy)imino)ethyl)-2H-chromen-2-one (**2**): Color: Colorless solid. Yield: 85%. M.p.: 154-157 °C. FT-IR (KBr, ν, cm^{-1}): 2849-3116 (C-H str.), 1746 (C=$O_{lactone}$ str.), 1726 (C=O_{ester} str.), 1623 (C=N str.), 1605 (C=C str.), 714 (N-O str.). ^{1}H NMR (400 MHz, $CDCl_3$, δ, ppm): 8.36 (s, 2H, Ar-H), 8.32 (s, 2H, Ar-H), 8.20 (s, 1H, Ar-H) 7.60 (d, 2H, *J* = 6.4 Hz, Ar-H), 7.35 (t, 2H, Ar-H), 2.58 (s, 3H, CH_3). ^{13}C NMR (100 MHz, $CDCl_3$, δ, ppm): 16.20 (CH_3), 163.83 (C=O_{ester}), 159.12 (C=$O_{lactone}$), 154.44 (C=N), 161.82, 150.90, 143.73, 134.17, 133.30, 130.90, 130.76, 129.17, 125.09, 123.90, 123.06, 118.41, 116.80 (Aromatic carbons). Anal. calcd. for $C_{18}H_{12}N_2O_6$: C, 61.37; H, 3.43; N, 7.95. Found: C, 61.33; H 3.42; N 7.89%.

3-(1-(((4-Methylbenzoyl)oxy)imino) ethyl)-2H-chromen-2-one (**3**): Color: Colorless solid. Yield: 65%. M.p.: 139-140 °C. FT-IR (KBr, ν, cm^{-1}): 2855-3114 (C-H str.), 1753 (C=$O_{lactone}$ str.), 1723 (C=O_{ester} str.), 1627 (C=N str.), 1608 (C=C str.), 741 (N-O str.). ^{1}H NMR (400 MHz, $CDCl_3$, δ, ppm): 8.20 (s, 1H, Ar-H), 8.01 (d, 2H, *J* = 6.8 Hz, Ar-H), 7.58 (d, 2H, *J* = 6.8 Hz, Ar-H), 7.27-7.37 (m, 4H, Ar-H), 2.55 (s, 3H, CH_3), 2.44 (s, 3H, *m*-CH_3). ^{13}C NMR (100 MHz, $CDCl_3$, δ, ppm): 16.03 (CH_3), 21.82 (*m*-CH_3), 163.68 (C=O_{ester}), 159.29 (C=$O_{lactone}$), 154.36 (C=N), 162.46, 144.55, 143.48, 133.00, 129.81, 129.67, 129.43, 129.32, 129.10, 128.58, 125.83, 124.98, 123.55, 118.56, 116.69 (Aromatic carbons). Anal. calcd. for $C_{19}H_{15}NO_4$: C, 71.02; H, 4.71; N, 4.36. Found: C, 71.00; H, 4.73; N, 4.31%.

3-(1-(((2-Chlorobenzoyl)oxy)imino) ethyl)-2H-chromen-2-one (**4**): Color: Colorless solid. Yield: 78%. M.p.: 142-143 °C. FT-IR (KBr, ν, cm^{-1}): 2847-3090 (C-H str.), 1763 (C=$O_{lactone}$ str.), 1718 (C=O_{ester} str.), 1627 (C=N str.), 1605 (C=C str.), 750 (N-O str.). ^{1}H NMR (400 MHz, $CDCl_3$, δ, ppm): 8.20 (s, 1H, Ar-H), 7.89 (d, 1H, *J* = 7.2 Hz, Ar-H), 7.29-7.62 (m, 7H, Ar-H), 2.52 (s, 3H, CH_3). ^{13}C NMR (100 MHz, $CDCl_3$, δ, ppm): 16.45 (CH_3), 163.27 (C=O_{ester}), 159.16 (C=$O_{lactone}$), 154.35 (C=N), 163.18, 143.62, 133.64, 133.15, 133.11, 131.66, 129.12, 129.00, 126.88, 125.02, 123.27, 118.47, 116.68 (Aromatic carbons). Anal. calcd. for $C_{18}H_{12}ClNO_4$: C, 63.26; H, 3.54; N, 4.10. Found: C 63.23; H 3.52; N 4.08%.

3-(1-(((4-Chlorobenzoyl)oxy)imino) ethyl)-2H-chromen-2-one (**5**): Color: Colorless solid. Yield: 82%. M.p.: 146-148 °C. FT-IR (KBr, ν, cm^{-1}): 2849-3094 (C-H str.), 1756 (C=$O_{lactone}$ str.), 1720 (C=O_{ester} str.), 1626 (C=N str.), 1607 (C=C str.), 746 (N-O str.). ^{1}H NMR (400 MHz, $CDCl_3$, δ, ppm): 8.19 (s, 1H, Ar-H), 8.06 (d, 2H, *J* = 7.6 Hz, Ar-H), 7.32-7.63 (m, 6H, Ar-H), 2.55 (s, 3H, CH_3). ^{13}C NMR (100 MHz, $CDCl_3$, δ, ppm): 16.07 (CH_3), 162.98 (C=O_{ester}), 159.21 (C=$O_{lactone}$), 154.40 (C=N), 162.80, 143.56, 140.22, 133.11, 131.13, 129.12, 127.10, 125.02, 123.35, 118.50, 116.74 (Aromatic carbons). Anal. calcd. for $C_{18}H_{12}ClNO_4$: C, 63.26; H, 3.54; N, 4.10. Found: C, 63.23; H, 3.56; N, 4.09%.

2.2. Single crystal X-ray crystallography

The analyzed crystal **1** has grown by slow evaporation method using ethanol as solvent. The crystal structure of compound **1** belongs to a monoclinic system with $P2_1/c$ symmetry. Details of the crystal data, data collection and refinement parameters for compound **1** are summarized in Table 1. Selected bond lengths, bond angles, and dihedral angles of compound **1** are given in Table 2. The ORTEP view of compound **1** with atomic labelling is shown in Figure 1, while Figure 2 shows the molecular packing arrangement in the unit cell. Determination of the unit cell parameters and data collection were performed on a Bruker 2008 SMART APEX II diffractometer using graphite-monochromated MoKα radiation (λ = 0.71073 Å) at 293 (2) K with a crystal of size 0.30 x 0.25 x 0.20 mm. Crystallographic data have been deposited with the Cambridge Crystallographic Data Centre as Supplementary Publication No. of compound **1** is CCDC 1036818.

2.3. Spectral measurements

FT-IR spectra of compounds **1-5** were acquired on an AVATAR-300 FT-IR spectrometer using KBr pellet. The spectral assignments are reported in wavenumber (cm^{-1}). FT-Raman spectra were recorded on a Bruker RFS 27: Stand-alone FT-Raman Spectrometer in solid state. The laser source used for the analysis is Nd: YAG 1064 nm. NMR spectra (^{1}H and ^{13}C) were recorded on a Bruker 400 MHz spectrometer. Chemical shift values are reported in parts per million (ppm) from tetramethylsilane (TMS).

Table 1. Crystal data and structural refinement for compound **1**.

Empirical formula	$C_{18}H_{13}NO_4$
Formula weight	307.29
Temperature (K)	293(2)
Crystal system	Monoclinic
Space group	$P2_1/c$
a (Å)	11.399(5)
b (Å)	5.876(5)
c (Å)	21.859(5)
β (°)	91.060(5)
Volume (Å^3)	1463.9(14)
Z	4
ρ_{calc} (g/cm^3)	1.394
μ (mm^{-1})	0.100
F(000)	640.0
Crystal size (mm^3)	0.30 × 0.25 × 0.20
Radiation	MoKα (λ = 0.71073)
2Θ range for data collection (°)	3.58 to 56.98
Index ranges	$-15 \le h \le 12$, $-7 \le k \le 7$, $-29 \le l \le 27$
Reflections collected	13555
Independent reflections	3669 [R_{int} = 0.0235]
Data/restraints/parameters	3669/0/209
Goodness-of-fit on F^2	1.022
Final R indexes [I≥2σ (I)]	R_1 = 0.0444, wR_2 = 0.1290
Final R indexes [all data]	R_1 = 0.0753, wR_2 = 0.1506
Largest diff. peak/hole (e Å^{-3})	0.18/-0.15

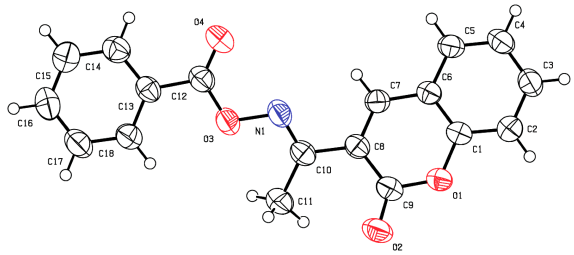

Figure 1. ORTEP view of compound **1**.

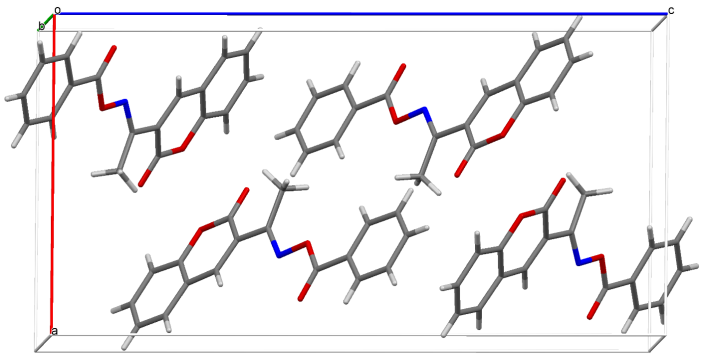

Figure 2. Packing diagram of compound **1**.

2.4. Computational details

Theoretical findings have been attained by B3LYP/6-311++G(d,p) technique using Gaussian 09W program package [23]. The hybrid function, Becke3 (B3) with Lee-Yang-Parr (LYP) correlation function [24,25], has been employed as a cost-effective approach. The optimized structures have been resolved by minimizing the energy with respect to all coordinates without imposing the molecular symmetry constraints. However, the optimized structural parameters have been used for further calculations like vibration frequency, electronic properties, and isotropic chemical shift. The frequency values computed at these levels contain known systematic errors. To bring the theoretical frequencies are in close proximity to the experimental values, the scaling factor values [26,27] of 0.96, 0.97, and 1.01 have been used for C-H, C-X stretching, bending, wagging, ring puckering and torsion vibrational frequencies, respectively. The chemical shifts have been computed at B3LYP/6-311++G(d,p) level using the Gauge Independent Atomic Orbital (GIAO) method [28].The ^{1}H and ^{13}C isotropic chemical shift values were referenced to the corresponding values of TMS, which was calculated at the same level of theory.

3. Results and discussion

3.1. Synthesis

The bio-pertinent 3-(1-((benzoyloxy)imino)ethyl)-2*H*-chromen-2-ones **1**-**5** has been synthesized by three-step synthetic protocol as outlined in Scheme 1.

Table 2. Selected structural parameters for compounds **1**-**5**.

Compound 1			Compound 2		Compound 3		Compound 4		Compound 5	
Bond lengths	**Calc. (Å)**	**Expt. (Å)** [a]	**Bond lengths**	**Calc. (Å)**	**Bond lengths**	**Calc. (Å)**	**Bond lengths**	**Calc. (Å)**	**Bond lengths**	**Calc. (Å)**
C1-C2	1.359	1.350 (19)	C1-C2	1.359	C1-C2	1.359	C1-C2	1.359	C1-C2	1.359
C1-C5	1.468	1.463 (2)	C1-C5	1.468	C1-C5	1.468	C1-C5	1.468	C1-C5	1.468
C1-C15	1.486	1.488 (2)	C1-C15	1.485	C1-C15	1.486	C1-C15	1.486	C1-C15	1.486
C2-C3	1.433	1.427 (2)	C2-C3	1.432	C2-C3	1.433	C2-C3	1.432	C2-C3	1.432
C3-C4	1.404	1.385 (2)	C3-C4	1.404	C3-C4	1.404	C3-C4	1.404	C3-C4	1.404
C3-C8	1.407	1.405 (19)	C3-C8	1.408	C3-C8	1.407	C3-C8	1.407	C3-C8	1.407
C4-C9	1.393	1.384 (2)	C4-C9	1.392	C4-C9	1.393	C4-C9	1.393	C4-C9	1.393
C4-O35	1.363	1.374 (16)	C4-O34	1.363	C4-O34	1.363	C4-O34	1.363	C4-O34	1.363
C5-O35	1.390	1.375 (19)	C5-O34	1.389	C5-O34	1.390	C5-O34	1.391	C5-O34	1.390
C5-O36	1.203	1.200 (2)	C5-O35	1.203	C5-O35	1.203	C5-O35	1.203	C5-O35	1.203
C8-C11	1.384	1.368 (2)	C8-C11	1.384	C8-C11	1.384	C8-C11	1.384	C8-C11	1.384
C9-C10	1.388	1.378 (2)	C9-C10	1.388	C9-C10	1.388	C9-C10	1.388	C9-C10	1.388
C10-C11	1.402	1.389 (2)	C10-C11	1.402	C10-C11	1.402	C10-C11	1.402	C10-C11	1.402
C15-C16	1.504	1.494 (2)	C15-C16	1.504	C15-C16	1.504	C15-C16	1.504	C15-C16	1.504
C15-N20	1.283	1.276 (2)	C15-N20	1.284	C15-N20	1.283	C15-N20	1.283	C15-N20	1.283
N20-O21	1.415	1.428 (17)	N20-O21	1.421	N20-O21	1.413	N20-O21	1.420	N20-O21	1.417
O21-C22	1.378	1.355 (2)	O21-C22	1.369	O21-C22	1.380	O21-C22	1.365	O21-C22	1.376
C22-O23	1.199	1.193 (18)	C22-O23	1.199	C22-O23	1.200	C22-O23	1.199	C22-O23	1.200
C22-C24	1.491	1.479 (2)	C22-C24	1.497	C22-C24	1.488	C22-C24	1.499	C22-C24	1.490
C24-C25	1.400	1.388 (2)	C24-C25	1.400	C24-C25	1.399	C24-C25	1.402	C24-C25	1.399
C24-C26	1.400	1.386 (2)	C24-C26	1.399	C24-C26	1.399	C24-C26	1.402	C24-C26	1.399
C25-C27	1.392	1.384 (2)	C25-C27	1.389	C25-C27	1.390	C25-C27	1.393	C25-C27	1.390
C26-C29	1.390	1.379 (2)	C26-C29	1.388	C26-C29	1.388	C26-C28	1.388	C26-C29	1.389
C27-C31	1.394	1.374 (3)	C27-C31	1.390	C27-C31	1.399	C27-C30	1.390	C27-C31	1.392
C29-C31	1.395	1.370 (2)	C29-C31	1.391	C29-C31	1.401	C28-C30	1.393	C29-C31	1.393
Bond angles	**(°)**	**(°)**	**Bond angles**	**(°)**	**Bond angles**	**(°)**	**Bond angles**	**(°)**	**Bond angles**	**(°)**
C2-C1-C5	120.1	119.1 (13)	C2-C1-C5	120.2	C2-C1-C5	120.1	C2-C1-C5	120.1	C2-C1-C5	120.1
C2-C1-C15	121.3	120.5 (14)	C2-C1-C15	121.4	C2-C1-C15	121.3	C2-C1-C15	121.3	C2-C1-C15	121.4
C5-C1-C15	118.4	120.2 (13)	C5-C1-C15	118.3	C5-C1-C15	118.4	C5-C1-C15	118.5	C5-C1-C15	118.4
C1-C2-C3	121.6	122.4 (14)	C1-C2-C3	121.5	C1-C2-C3	121.6	C1-C2-C3	121.6	C1-C2-C3	121.6
C2-C3-C4	117.5	117.6 (13)	C2-C3-C4	117.5	C2-C3-C4	117.5	C2-C3-C4	117.6	C2-C3-C4	117.5
C2-C3-C8	123.8	123.9 (14)	C2-C3-C8	123.8	C2-C3-C8	123.8	C2-C3-C8	123.8	C2-C3-C8	123.8
C4-C3-C8	118.5	118.3 (14)	C4-C3-C8	118.5	C4-C3-C8	118.5	C4-C3-C8	118.5	C4-C3-C8	118.5
C3-C4-C9	121.4	121.8 (13)	C3-C4-C9	121.4	C3-C4-C9	121.4	C3-C4-C9	121.4	C3-C4-C9	121.4
C3-C4-O35	120.8	120.5 (13)	C3-C4-O34	120.8	C3-C4-O34	120.8	C3-C4-O34	120.8	C3-C4-O34	120.8
C9-C4-O35	117.7	117.6 (13)	C9-C4-O34	117.6	C9-C4-O34	117.7	C9-C4-O34	117.7	C9-C4-O34	117.7
C1-C5-O35	116.2	117.0 (12)	C1-C5-O34	116.2	C1-C5-O34	116.2	C1-C5-O34	116.2	C1-C5-O34	116.2
C1-C5-O36	126.3	127.1 (15)	C1-C5-O35	126.2	C1-C5-O35	126.3	C1-C5-O35	126.3	C1-C5-O35	126.3
O35-C5-O36	117.4	115.8 (14)	O34-C5-O35	117.5	O34-C5-O35	117.3	O34-C5-O35	117.4	O34-C5-O35	117.4
C3-C8-C11	120.4	120.2 (15)	C3-C8-C11	120.3	C3-C8-C11	120.4	C3-C8-C11	120.4	C3-C8-C11	120.4
C4-C9-C10	118.8	118.4 (15)	C4-C9-C10	118.7	C4-C9-C10	118.8	C4-C9-C10	118.8	C4-C9-C10	118.8
C9-C10-C11	120.8	120.9 (15)	C9-C10-C11	120.8	C9-C10-C11	120.8	C9-C10-C11	120.8	C9-C10-C11	120.8
C8-C11-C10	119.8	120.1 (14)	C8-C11-C10	119.8	C8-C11-C10	119.8	C8-C11-C10	119.8	C8-C11-C10	119.8
C1-C15-C16	121.1	122.5 (14)	C1-C15-C16	121.1	C1-C15-C16	121.1	C1-C15-C16	121.2	C1-C15-C16	121.1
C1-C15-N20	113.3	112.4 (13)	C1-C15-N20	113.2	C1-C15-N20	113.3	C1-C15-N20	113.1	C1-C15-N20	113.3
C16-C15-N20	125.4	125.0 (15)	C16-C15-N20	125.5	C16-C15-N20	125.4	C16-C15-N20	125.5	C16-C15-N20	125.5
C15-N20-O21	110.8	110.2 (12)	C15-N20-O21	110.6	C15-N20-O21	110.9	C15-N20-O21	110.6	C15-N20-O21	110.8
N20-O21-C22	113.2	112.5 (11)	N20-O21-C22	113.1	N20-O21-C22	113.2	N20-O21-C22	113.3	N20-O21-C22	113.1
O21-C22-O23	124.1	123.9 (15)	O21-C22-O23	124.9	O21-C22-O23	123.9	O21-C22-O23	125.0	O21-C22-O23	124.3
O21-C22-C24	110.5	110.7 (13)	O21-C22-C24	110.4	O21-C22-C24	110.5	O21-C22-C24	110.7	O21-C22-C24	110.5
O23-C22-C24	125.3	125.2 (16)	O23-C22-C24	124.6	O23-C22-C24	125.4	O23-C22-C24	124.0	O23-C22-C24	125.1
C22-C24-C25	122.8	122.9 (15)	C22-C24-C25	122.7	C22-C24-C25	123.1	C22-C24-C25	126.0	C22-C24-C25	123.0
C22-C24-C26	117.4	117.7 (14)	C22-C24-C26	117.2	C22-C24-C26	117.7	C22-C24-C26	115.6	C22-C24-C26	117.5
C25-C24-C26	119.6	119.3 (15)	C25-C24-C26	119.9	C25-C24-C26	119.1	C25-C24-C26	118.2	C25-C24-C26	119.4
C24-C25-C27	119.9	119.9 (17)	C24-C25-C27	120.1	C24-C25-C27	120.1	C24-C25-C27	120.6	C24-C25-C27	120.4
C24-C26-C29	120.1	120.1 (15)	C24-C26-C29	120.3	C24-C26-C29	120.3	C24-C26-C28	121.3	C24-C26-C29	120.6
C25-C27-C31	120.1	120.1 (16)	C25-C27-C31	118.6	C25-C27-C31	121.2	C25-C27-C30	120.0	C25-C27-C31	119.1
C26-C29-C31	120.0	120.2 (17)	C26-C29-C31	118.5	C26-C29-C31	121.0	C26-C28-C30	119.5	C26-C29-C31	119.0
C27-C31-C29	120.0	120.2 (17)	C27-C31-C29	122.3	C27-C31-C29	118.1	C27-C30-C28	120.1	C27-C31-C29	121.3
C4-O35-C5	123.4	123.1 (12)	C4-O34-C5	123.4	C4-O34-C5	123.4	C4-O34-C5	123.4	C4-O34-C5	123.4

The key component, 3-acetyl-2*H*-chromen-2-one has synthesized by Knoevenagel condensation of salicylaldehyde with ethyl acetoacetate in 1:1 molar ratio followed by oximation using hydroxylamine hydrochloride in the presence of sodium acetate trihydrate in ethanol gave 3-(1-(hydroxyimino)ethyl)-2*H*-chromen-2-one in good yields. In the eventual step, bio-pertinent 3-(1-((benzoyloxy)imino)ethyl)-2*H*-chromen-2-ones **1**-**5** have been synthesized from 3-(1-(hydroxyimino)ethyl)-2*H*-chromen-2-one with benzoic acid using $POCl_3$ [29] and pyridine as solvent as well as base afforded the corresponding oxime esters **1**-**5** in good yields.

3.2. Molecular geometry

From the single crystal XRD measurements of compound **1**, both the pyrone and benzene rings in the coumarin motif are essentially planar, which is evidenced by the dihedral angle value between their carbons C2-C3-C4-C9 [178.9(13)°]. The imino (C=N) group of oxime ester adopts an *anti-orientation* relative to the C=C double bond [C1-C15-N20-O21 178.0 (11)°]. Thus, the molecule is about C-C=N bond which is found to exist in *E*-isomer with respect to the olefinic C=C bond. In addition, the bond angles of the imino group *versus* the coumarin moiety and methyl group are 112.4(13)°, 125.0(15)° [C-C=N], respectively. These values are emblematic of the angle permitted by the rotation present at position 3. Presence of the imino group at position 3 provokes a non-coplanarity of the oxime ester moiety relative to the parent coumarin.

The optimized structural features (bond lengths, bond angle, and dihedral angles) for thermodynamically preferred geometry of compounds **1**-**5** were computed at B3LYP/6-311++G(d,p) level.

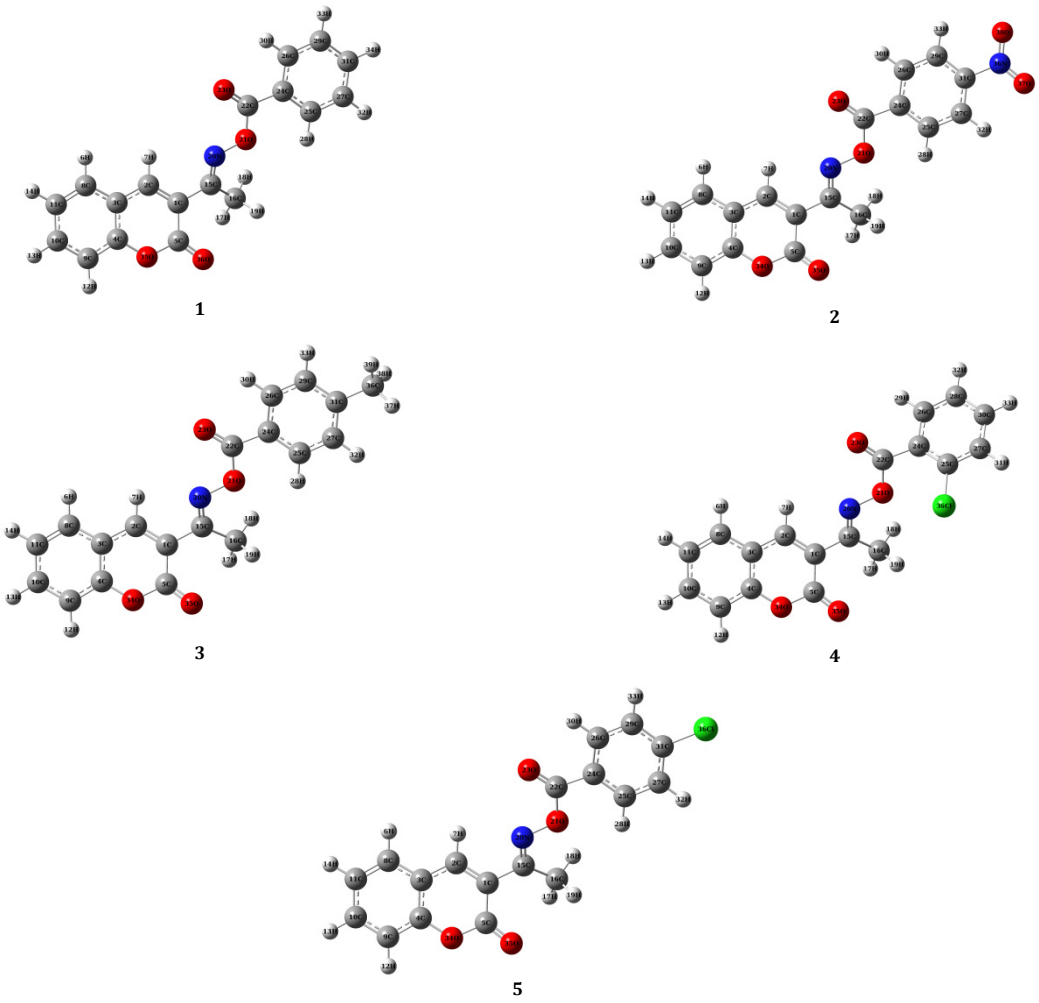

Figure 3. Optimized geometry and atom numbering of compounds **1-5**.

Theoretically, resulted structural parameters were compared with the single crystal XRD values of compound **1**. The optimized structures for compounds **1-5** are shown in Figure 3. The mean C-H bond lengths of compounds **1-5** are 1.08 Å, in good agreement with the experimental value of C-H bond [30, 31]. Bond lengths connecting to the ring carbons are found to be around 1.38-1.40 Å, which is in-line with the expected range of title molecule, 1.368-1.407 Å. The computed bond angles of sp^2hybrids of ring carbons are around 120°. Double bond length of carbon-nitrogen, carbon-oxygen and single bond length of carbon-oxygen, nitrogen-oxygen are about 1.28, 1.20, 1.37, and 1.41 Å, respectively, which are found to coincide with their experimental results [32].

The side chain, 3-acetyl part of compounds **1-5** are bonded to the C1 atom of the coumarin ring. The geometry of the coumarin ring is planar as indicated by C2-C3-C4-C9 (-179.2°) and C8-C3-C4-O35 (-179.9°) which are matched with the experimental values and are listed in Table 2. The dihedral angles C2-C1-C15-C16 (-141.9°, -141.7°, -142.1°) and C2-C1-C15-N20 (36.1°, 36.4°, 35.9°, 36.0) indicate that the 3-acetyl part deviated from the coumarin ring *i.e.* the 3-acetyl part lies in other plane.

3.3. Vibrational analysis

The combined experimental and theoretically simulated Infra-red and Raman spectra of the compounds **1** under investigation are shown in Figure 4. The experimental and theoretically computed frequencies along with their relative intensities, probable assignments, and potential energy distribution (PED) of compound **1** are summarized in Table 3. The hypothetically computed frequencies of the studied compounds **1-5** are in accord with the experimental ones.

3.3.1. C=O and C-O vibrations

Compounds possessing carbonyl groups give a strong absorption in the region of 1650-1750 cm^{-1} [33-36]. In compounds **1-5**, the distinctive FT-IR bands emerged at 1694-1726 and 1739-1763 cm^{-1} which confirmed the presence of carbonyl groups, while in FT-Raman absorption bands have been appeared at 1713-1724 and 1739-1759 cm^{-1}. The computed carbonyl (C=O) stretching vibrations of ester and lactone carbonyl are at 1734-1759 and 1731-1735 cm^{-1} which correlated well with the experimental ones. The variations of stretching frequency of the carbonyl group are due to the presence of different substitutions on the phenyl ring in the compounds.

The stretching frequency of C-O appeared in the region of 1150-1280 cm^{-1} [34,35]. In the present study, the bands appeared at 1215-1268 and 1317-1348 cm^{-1} in FT-IR and at 1210-1268 and 1320-1335 cm^{-1} in FT-Raman are due to the C-O stretching vibration of the synthesized compounds **1-5**. The computed FT-IR and FT-Raman spectral values (1197-1286 and 1313-1336 cm^{-1}) are coincided well with the experimental results.

Table 3. Experimental and calculated vibrational (FT-IR and Raman) spectral values of compound **1** with their proposed vibrational assignments.

Mode no	Exp. frequency (cm^{-1})		Calc. frequency (cm^{-1})				Vibrational assignments with PED ≥ 10% *
	FT-IR	FT-Raman	Unscaled	Scaled	I_{IR}	I_{Raman}	
1			10	10	5.26	3.83	γC3C9O35C4(12)
2			28	28	8.44	5.60	γC15C2C5C1(12); τC15C1C5O35(20)
3			33	33	2.79	6.59	γC22C24C26C25(12)
4			49	49	3.22	13.35	γC16C1N20C15(12)
5			71	72	3.11	7.99	γO23C24O21C22(12)
6			90	91	5.16	3.76	γO36C1O35C5(12); τC4O35C5O36(20)
7			109	110	3.82	3.22	τC1C15N20O21(20)
8			111	112	3.17	5.11	τC24C22O21N21(20)
9			159	161	3.27	3.84	τC1C4C5O35(20)
10			170	172	3.28	5.17	τC15N20O21C22(20)
11			187	189	3.85	6.32	τC26C24C22O21(20)
12			212	214	2.10	3.17	γC11C8C9C10(12)
13			236	238	8.23	5.43	τC27C25C31C29(20)
14			262	265	9.79	7.04	τC26C29C27C31(20)
15			309	312	7.11	2.53	τC24C26C31C29(18)
16			322	325	1.94	3.30	γC9C10O35C4(12); τC9C10C4O35(20)
17			327	330	7.77	8.39	γC10C4C11C9(26)
18			371	375	7.79	3.66	γC8C3C10C11(24)
19		393	386	390	4.07	5.77	τC1C5C2C3(22)
20	417		411	415	2.28	2.91	τC2C1C15N20(25)
21	432		421	425	8.82	7.50	τH34C31C29C26(28)
22	456	450	455	460	6.48	17.9	τH19C16C15C1(18); γC16H18C15H19(12)
23	478	477	466	471	8.62	5.30	τH33C29C31C29(32)
24			480	485	2.45	6.13	τH32C27C31C29(30)
25		496	494	499	8.87	4.92	τH30C26C29C31(38)
26	539	536	548	553	3.23	4.44	τH28C25C27C31(15); γC25C24C27H28(18)
27	556	563	565	571	5.91	2.21	τH18C16C15C1(18); γC16H17C15H18(15)
28	589	586	585	591	9.93	9.91	τH17C16C15C1(20); γC16H18H19H17(10)
29	616	609	608	614	14.2	4.98	τH14C11C10C9(44)
30	635	634	631	637	6.86	10.66	τH13C10C11C8(16); τH13C10C9C4(20)
31			644	650	13.93	5.76	τH12C9C10C11(20)
32	670	674	669	676	33.65	8.03	τH6C8C11C10(18); γH6C11C3C8(20)
33	683		673	680	6.61	8.14	τH7C2C1C5(24)
34	701	699	701	708	17.21	2.60	βC15N20O21(22); γC8C3O35C4(15)
35			718	725	33.65	5.28	βC16C15N20(25); βC1C15C16(10)
36	739	737	746	753	6.95	8.61	βC24C22O21(38)
37			752	760	4.61	26.83	βC4O35C5(42)
38	772	779	770	778	38.03	2.62	βC5C1C15(28); βC2C1C15(14)
39			779	787	17.70	9.89	βC22O21N20(40)
40	800		791	799	9.25	7.41	βC22C24C26(35)
41	822	817	812	820	11.79	6.02	βC8C11C10(33)
42		854	848	856	11.86	12.37	βC25C27C31(38)
43	868	871	858	867	6.26	5.03	βC27C31C29(25)
44			875	884	6.78	1.81	βC26C29C31(26)
45	922	915	931	940	42.01	16.50	βC4C9C10(30)
46		944	939	948	53.33	10.84	βC9C10C11(26)
47			952	962	10.44	5.88	βC3C8C11(28)
48	968		956	966	27.01	6.68	βC2C1C5(38)
49			976	986	20.38	6.88	βC1C15N20(32)
50	991	999	986	996	53.22	16.03	βO35C5O36(15); βC1C5O36(25)
51			993	1003	4.08	0.61	βO21C22O23(18); βC24C22O23(10)
52			1000	1010	2.71	1.90	βH34C31C29(22); βH34C31C27(12)
53			1010	1020	0.64	1.12	βH18C16H19(19); βH17C16H19(21)
54	1024	1024	1018	1028	2.50	28.90	βH33C29C31(20); βH33C29C26(20)
55			1039	1049	28.19	30.38	βH32C27C31(22); βH32C27C25(18)
56	1055	1051	1046	1056	16.97	19.56	βH30C26C29(25); βH30C26C24(12)
57			1051	1062	10.05	17.60	βH28C25C27(28); βH28C25C24(15)
58	1078	1074	1061	1072	5.89	10.09	βH17C16H18(26); βH18C16C15(10)
59	1100		1073	1084	55.08	12.30	βH17C16H19(32); βH17C16C15(14)
60	1125	1129	1110	1121	9.19	9.59	βH14C11C8(25); βH14C11C10(12)
61			1132	1143	30.79	18.54	βH13C10C11(28); βH13C10C9(15)
62			1146	1157	14.16	6.70	βH12C9C10(32); βH12C9C4(10)
63			1183	1195	14.04	11.14	βH6C8C11(30); βH6C8C3(22)
64			1184	1196	3.26	9.19	βH7C2C1(38); βH7C2C3(10)
65	1159	1160	1205	1169	22.06	6.89	νN20O21(35); βC4C3C8(18)
66	1176	1181	1238	1188	64.96	22.37	νC15C16(42)
67			1247	1197	35.14	46.05	νC22C24(44)
68	1215	1215	1271	1233	49.81	34.72	νC5O35(40)
69		1238	1284	1233	38.78	3.84	νC1C15(48)
70	1249	1263	1321	1281	22.69	12.49	νC22O21(52)
71			1334	1281	6.59	2.32	νC1C5(41); βC1C5O35(25)
72	1317		1354	1313	6.14	7.15	νC4O35(42); βC9C4O35(28)
73			1365	1310	5.73	47.22	νC2C3(44); βC1C2C3(26)
74	1320	1330	1389	1333	10.25	14.88	νC3C8(40); βC2C3C8(35)
75	1373	1362	1405	1349	20.75	11.84	νC24C25(45); βC25C24C26(30)
76			1474	1415	13.09	12.00	νC24C26(50); βC24C26C29(28)
77			1477	1418	15.88	5.37	νC10C11(66)
78			1482	1423	18.55	21.48	νC3C4(58)
79			1485	1426	17.21	25.57	νC27C31(60)

Table 3. Continued.

Mode no	Exp. frequency (cm^{-1})		Calc. frequency (cm^{-1})				Vibrational assignments with PED ≥ 10% *
	FT-IR	FT-Raman	Unscaled	Scaled	I_{IR}	I_{Raman}	
80	1450	1446	1515	1454	11.46	30.89	νC29C31(62)
81	1488	1490	1522	1461	5.48	5.32	νC27C27(55); βC24C25C27(30)
82			1599	1535	35.29	85.48	νC26C29(66)
83	1556	1555	1620	1555	8.21	11.64	νC4C9(68)
84			1640	1574	16.74	38.17	νC9C10(75)
85	1582		1646	1580	36.33	74.25	νC8C11(72)
86	1604	1601	1653	1587	40.00	100.00	νC1C2(78)
87	1622		1674	1624	13.38	62.13	νC15N20(70)
88	1694	1716	1786	1732	100.00	32.58	νC5O36(75)
89	1739	1745	1791	1737	66.44	50.51	νC22O23(80)
90	2849	2919	3036	2915	13.70	59.36	νC31H34(82)
91	2925	2984	3105	2981	10.91	36.24	νC16H19(80)
92	3009	2997	3141	3015	8.26	37.60	νC29H33(88)
93	3039	3037	3166	3039	1.92	30.25	νC27H32(85)
94			3174	3047	1.04	23.87	νC26H30(89)
95			3178	3051	11.89	45.42	νC25H28(91)
96			3182	3055	8.66	42.28	νC16H18(94)
97	3064	3064	3188	3060	16.99	51.75	νC16H17(90)
98			3196	3068	12.35	48.73	νC11H14(92)
99			3198	3070	4.97	33.88	νC10H13(96)
100			3199	3071	11.36	49.90	νC9H12(95)
101		3226	3205	3077	7.90	66.24	νC8H6(100)
102	3090	3245	3214	3085	7.37	42.00	νC2H7(98)

* ν - stretching, β - inplane bending, γ - out of plane bending, τ - torsional vibrations.

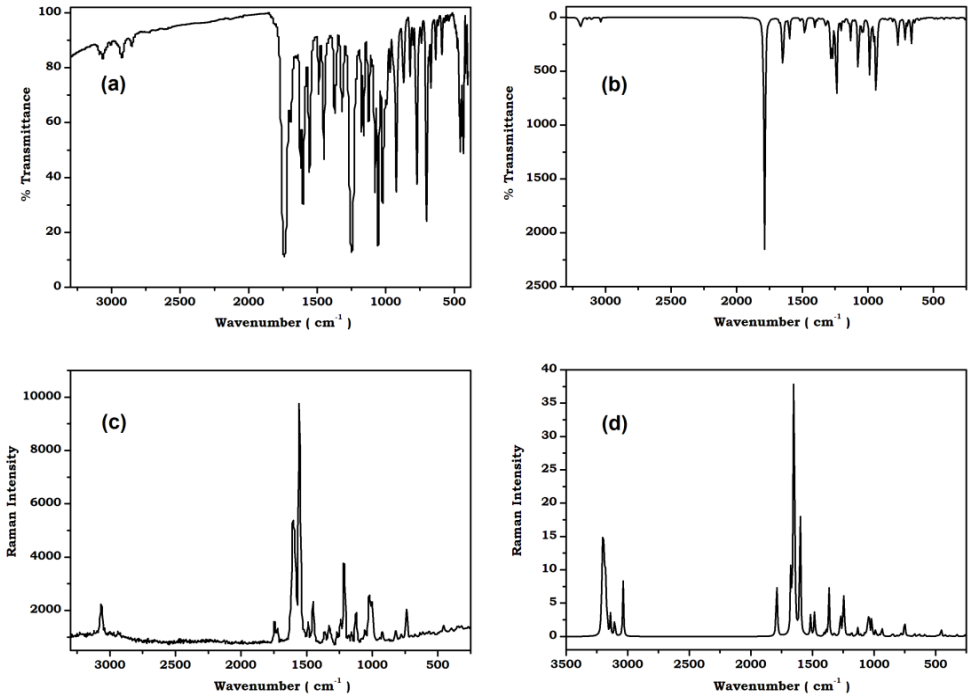

Figure 4. (**a**) FT-IR spectrum of compound **1**, (**b**) Simulated FT-IR spectrum of compound **1**, (**c**) FT-Raman spectrum of compound **1**, (**d**) Simulated FT-Raman spectrum of compound **1**.

3.3.2. C=N and N-O vibrations

Oxime esters containing C=N and N-O bonds show characteristic bands in the region 1620-1690 and 945 cm^{-1} [37]. In the present case, the peaks appeared in the region of 1622-1627 and 1134-1165 cm^{-1} in FT-IR (1606-1687 and 1133-1160 cm^{-1} in FT-Raman) are assigned to C=N and N-O stretching vibrations. The calculated wave numbers of C=N and N-O stretching vibrations (1622-1631 and 1141-1169 cm^{-1}) coincided with their experimental values.

3.3.3. C=C and C-C vibration

The aromatic carbon-carbon stretching frequencies (C=C and C-C) generally arise in the region from 1480 to 1630 cm^{-1} [38-40]. In our present study, the frequencies occur in FT-IR at 1249-1608 cm^{-1} and in FT-Raman 1255-1612 cm^{-1} are owing to the carbon-carbon stretching modes. The theoretically calculated frequencies at 1268-1589 cm^{-1} by DFT method are well coincided with the experimental values. The C-C-C in-plane and out-of-plane bending modes of compound **1** is presented in Table 3.

3.3.4. C-H vibration

The aromatic and heteroaromatic C-H stretching bands are typically occurring below 3100 cm^{-1} [41,42]. In accordance with this, the absorption bands at 3031-3116 cm^{-1} in FT-IR spectrum and 3037-3245 cm^{-1} in FT-Raman spectrum are assigned to the C-H stretching frequency of the studied molecules. The calculated C-H stretching frequencies (3036-3099 cm^{-1}) agreed well with the observed frequencies.

Table 4. Mulliken atomic charges of compounds **1**-**5**.

1		2		3		4		5	
Atom	**Charge**	**Atom**	**Charge**	**Atom**	**Charge**	**Atom**	**Charge**	**Atom**	**Charge**
1C	0.3930	1C	0.3799	1C	0.3503	1C	0.3973	1C	0.3836
2C	0.1149	2C	0.1243	2C	0.1388	2C	0.2270	2C	0.1197
3C	1.5905	3C	1.5959	3C	1.5858	3C	1.6767	3C	1.5904
4C	-1.9272	4C	-1.9162	4C	-1.9292	4C	-1.9667	4C	-1.9095
5C	0.0043	5C	0.0069	5C	0.0102	5C	-0.0991	5C	0.0111
6H	0.1532	6H	0.1534	6H	0.1531	6H	0.1529	6H	0.1531
7H	0.2430	7H	0.2425	7H	0.2445	7H	0.2335	7H	0.2446
8C	0.1599	8C	0.1538	8C	0.1671	8C	0.1874	8C	0.1486
9C	-0.3738	9C	-0.3847	9C	-0.3718	9C	-0.3588	9C	-0.3888
10C	-0.3419	10C	-0.3418	10C	-0.3446	10C	-0.3418	10C	-0.3425
11C	-0.1521	11C	-0.1483	11C	-0.1499	11C	-0.1542	11C	-0.1476
12H	0.2059	12H	0.2076	12H	0.2056	12H	0.2067	12H	0.2062
13H	0.1768	13H	0.1791	13H	0.1764	13H	0.1770	13H	0.1776
14H	0.1745	14H	0.1765	14H	0.1743	14H	0.1749	14H	0.1751
15C	0.2115	15C	0.2204	15C	0.2106	15C	0.0917	15C	0.2123
16C	-0.8236	16C	-0.8257	16C	-0.8168	16C	-0.8207	16C	-0.8192
17H	0.1881	17H	0.1918	17H	0.1878	17H	0.1856	17H	0.1896
18H	0.1828	18H	0.1819	18H	0.1831	18H	0.1827	18H	0.1819
19H	0.2209	19H	0.2239	19H	0.2204	19H	0.2192	19H	0.2221
20N	-0.2842	20N	-0.2858	20N	-0.2870	20N	-0.2717	20N	-0.2847
21O	0.2946	21O	0.2984	21O	0.2916	21O	0.3630	21O	0.2858
22C	-0.4337	22C	-0.2601	22C	-0.3636	22C	-1.0307	22C	-0.4966
23O	-0.1855	23O	-0.1737	23O	-0.1861	23O	-0.1618	23O	-0.1854
24C	0.9850	24C	1.1426	24C	1.1591	24C	0.3054	24C	0.9388
25C	-0.2122	25C	-0.2362	25C	-0.5008	25C	0.4436	25C	-0.4375
26C	-0.0464	26C	-0.1368	26C	-0.1905	26C	-0.0102	26C	-0.1841
27C	-0.3760	27C	-0.5543	27C	-0.6363	27C	-0.3232	27C	-0.6539
28H	0.1515	28H	0.1813	28H	0.1278	28H	-0.1987	28H	0.1490
29C	-0.4879	29C	-0.4170	29C	-0.5536	29C	0.1979	29C	-0.6756
30H	0.2006	30H	0.2192	30H	0.1904	30C	-0.4072	30H	0.2059
31C	-0.1719	31C	-0.1581	31C	0.6036	31H	0.2065	31C	0.3794
32H	0.1843	32H	0.2545	32H	0.1763	32H	0.1776	32H	0.2106
33H	0.1735	33H	0.2515	33H	0.1634	33H	0.1636	33H	0.1988
34H	0.1604	34O	-0.0914	34O	-0.0949	34O	-0.0946	34O	-0.0936
35O	-0.0941	35O	-0.2573	35O	-0.2587	35O	-0.2551	35O	-0.2584
36O	-0.2590	36N	-0.2247	36C	-0.5026	36Cl	0.5241	36Cl	0.4933
		37O	0.0169	37H	0.1465				
		38O	0.0094	38H	0.1733				
				39H	0.1462				

The weak-medium-strong peaks seen at 911-1250 and 387-553 cm^{-1} in FT-IR spectra and 909-1236 and 414-536 cm^{-1} in FT-Raman spectra are due to the effect of C-H in-plane and out-of-plane bending vibrations, respectively [43]. The in-plane and out-of-plane bending vibrations of the C-H bonds have also been identified for the synthesized compounds **1**-**5** and they agreed with the calculated frequencies as shown in Table 3.

3.3.5. Methyl group vibration

The C-H stretching in alkyl groups are clearly obtained at lower frequencies than those of aromatic ring vibrations, *i.e.*, 2970-2840 cm^{-1} [44-46]. The weak and medium bands for CH_3 stretching frequencies are occurred in FT-IR at 2786-3021 cm^{-1} and in FT-Raman at 2866-3013 cm^{-1}, whereas the calculated stretching frequencies are 2902-3016 cm^{-1}.

The deformation vibrations of CH_3 at 1471-1487, 1019-1089, and 556-680 cm^{-1} in FT-IR and in FT-Raman at 1488-1491, 1074-1089 and 563-678 cm^{-1} are assigned to the mixture deformation modes with C-H and skeleton vibrations. All characteristic assignments obtained from experimental and calculated ones are well synchronized with literature values [47].

3.3.6. Nitro group vibration

Typically, the nitro group stretching frequencies are exhibited as the same as in the C-C stretching regions. The deformation vibrations of NO_2 group (rocking, wagging, and twisting) contribute to several normal modes in the low frequency region [48]. In compound **2**, the very strong bands observed in FT-IR at 1370 cm^{-1} and in FT-Raman at 1351 cm^{-1} are assigned to stretching vibrations of the nitro group and agree well with the observed band at 1331 cm^{-1}.

3.3.7. C-Cl vibrations

The vibration frequencies belonging to CX groups (X = Cl, Br, and I) usually occurred in the frequency range of 850-500 cm^{-1} with more than one halogen atom exhibiting very strong bands due to asymmetric and symmetric stretching modes [43]. In the FT-IR spectra of compounds **4** and **5** the absorption zones at 689 and 694 cm^{-1} whereas in FT-Raman at 692 and 710 cm^{-1} are assigned to C-Cl stretching vibrations of the molecule. The calculated wave numbers of C-Cl stretching bands arising at 708 and 703 cm^{-1} by B3LYP/6-311++G (d,p) coincided very well with the experimental value. The band at 474 cm^{-1} for compound **4** and at 525 cm^{-1} for compound **5** in FT-IR are assigned to the C-Cl torsion mode of vibration.

3.4. Mulliken population analysis

The atomic charges of an individual atom are determined *via* Mulliken population analysis. Mulliken electron populations of compounds **1**-**5** have been acquired from the optimized structural calculation and the values are collected in Table 4. The charge distributions over the atoms suggest the formation of donor and acceptor pairs involving the charge transfer in the molecule [49]. In compounds **1**-**5**, the magnitude of carbon (3C) atom has gained higher positive charge and becomes more acidic, while carbon (4C) has high negative charge than the other atoms due to the fusion of benzene ring and pyrone ring through a more electronegative oxygen atom.

Table 5. Calculated HOMO-LUMO energies of compounds **1**-**5**.

Parameters	1	2	3	4	5
E_{HOMO}	-8.4261	-8.4416	-8.4168	-8.4241	-8.4114
E_{LUMO}	-5.5596	-5.5830	-5.5542	-5.5501	-5.5498
ΔE	2.8665	2.8586	2.8626	2.8740	2.8616
E_{HOMO-1}	-9.0585	-9.0655	-9.0500	-8.9162	-8.9227
E_{LUMO+1}	-5.0589	-5.3218	-4.9756	-4.8570	-4.8899
ΔE_1	3.9996	3.7437	4.0744	4.0592	4.0328

All hydrogen and carbon atoms in the coumarin and ester fragments are carrying positive and negative charges, respectively. Besides, 3C and 24C are holding positive charges. The results suggest that the electron delocalization takes place in the entire molecule [50].

3.5. NBO analysis

Natural bond orbital (NBO) analysis grants a new approach to studying natural charges, bond types, bond order, charge transfer, and donor-acceptor interactions in a molecule [51-53]. The hyper-conjugative interaction energy of a molecule was deduced from the second order perturbation approach (SOPT).

$$E^{(2)} = \Delta E_{ij} = q_i \frac{F(i,j)^2}{\varepsilon_j - \varepsilon_i} \quad (1)$$

where q_i is the donor orbital occupancy, ε_i and ε_j are diagonal elements, and F(i,j) is the off-diagonal NBO Fock matrix element.

The SOPT analysis of Fock matrix of compounds **1**-**5** has been carried out with B3LYP/6-311++G(d,p) method. For convenience, compound **1** has been selected for discussion. The significant interactions between bond and antibonding orbitals with lone pair electrons and their corresponding $E^{(2)}$ of the molecule were observed. An effective interaction has been observed between the lone pair of electrons on oxygen (O23 and O35) and the antibonding orbitals of coumarin and benzoyl parts. These interactions are formed by the orbital overlap between bonding and antibonding orbitals, which result in intramolecular charge transfer (ICT) causing stabilization of the molecule. The stabilization energy $E^{(2)}$ of n(O21) → π*(C22-O23), n(O23) → σ*(O21-C22), n(O35) → π*(C3-C4), n(O35) → π*(C5-O36), n(O36) → π*(C5-O35), π*(C3-C4) → π*(C1-C2), π*(C3-C4) → π*(C8-C11), π*(C5-O36) → π*(C1-C2),) π*(C27-C31) → π*(C29-H33) are 37.17, 37.47, 28.97, 35.5, 35.64, 184.22, 259.02, 84.35 and 28.82 kcal/mol. High $E^{(2)}$ values indicate that the strong interaction observed between electron donor and acceptors which results in extended conjugation occurs in the molecular system. Moreover, the higher values of $E^{(2)}$ are chemically significant and have been used as to measure the intermolecular hydrogen bonding (C-H---O) interaction between the lone pair of oxygen and the antibonding orbitals. The electron density of six conjugated π bonds (~1.6) and π* bond (~0.3) in the benzoyl group and benzene ring of coumarin have clearly demonstrated strong delocalization. The stabilization energies of π→π* electrons in benzoyl group and in benzene ring are 17.05, 18.73, 15.98, 17.59 21.13, 22.38, 16.92, 20.18, 20.55, 19.26, 22.53 and 18.12 kcal/mol.

The stabilization energies of π→π* electrons in compounds **2**-**5** are higher than compound **1** and the antibonding interactions between the lone pair of electrons are higher, which reveal that compounds **2**-**5** form intramolecular charge transfer which leads to a greater extent of conjugation in the molecule.

3.6. HOMO-LUMO analysis

From the optimized structural calculation, HOMO, LUMO and band gap energies of compounds **1**-**5** were determined and 3D plots of compounds **1**-**5** are shown in Figure 5. The color codes, red and green designate the positive and negative phases of the molecules. The energy gap between HOMO and LUMO of compounds **1**-**5** decreases in the order: **2** > **5** > **3** > **1** > **4** and the values are tabulated in Table 5. From Figure 5, the HOMO of molecular charges is spread over the coumarin ring and imino group, while the LUMO implies a slight electron density transfer from the coumarin ring to the oxime ester part, which increases the molecular polarity of compounds **1**-**5**. Among compounds **1**-**5**, compound **2** has the minimum energy gap which results in the eventual charge transfer taking place within the molecule due to the presence of an electronegative group in the molecule. Furthermore, the HOMO-LUMO energy gap of compounds **1**-**5** are compared with their corresponding coumarin derivatives [34,35,54-56] like 3-acetyl-2*H*-chromen-2-one (4.176 eV), 3-(1-(((methoxycarbonyl)oxy) imino)ethyl)-2*H*-chromen-2-one (4.244 eV), (*Z*)-*N*-Cyclohexyl-2-(2-((2-oxo-2*H*-chromen-3-yl)-methoxy)benzylidene)hydrazinecarbothioamide (3.053 eV), (*Z*)-*N*-(2, 4-Dimethylphenyl)-2-(2-((2-oxo-2*H*-chromen-3-yl)methoxy)benzylidene)hydrazinecarbo-thioamide (3.118 eV) 7-hydroxy-2*H*-chromen-2-one (4.420 eV) and 3-cyano-4-methyl-2*H*-chromen-2-one (4.292 eV), the compounds **1**-**5** are found to have lesser energy gap than the above mentioned compounds due to the introduction of oxime ester into the 3-acetyl part.

3.7. NMR spectral analysis

The ^{1}H and ^{13}C chemical shifts of compounds **1**-**5** have been calculated by B3LYP/6-311++G(d,p) method. A sharp singlet with three protons integrals resonated in the shielded region at ~2.5 ppm corresponding to the presence of methyl protons (17H, 18H, and 19H) of compounds **1**-**5** and the values are matched well with the computed chemical shifts. The signal of olefinic proton 7H of compounds **1**-**5** appeared to be shielded by 0.25 ppm with respect to the parent 3-acetyl-2*H*-chromen-2-one [34]. The same 7H proton signal was deshielded by 0.13 ppm with respect to 3-(1-(((methoxycarbonyl)oxy)-imino) ethyl)-2*H*-chromen-2-one [35]. This suggests a weakening/ strengthening of the π-π conjugation between the lactone carbonyl and the imino group. The aromatic protons of coumarin and *o*-benzoyl groups are seen in the downfield region from 7.29 to 8.36 ppm.

The aromatic carbon signals are generally arising in the range from 100 to 160 ppm in organic molecules [57]. In the present study, the aromatic carbons fall in the down field region 116-154 ppm, which are in accord with the computed ones. The signals appeared in the up field from 16.03-16.45 ppm corresponding to the methyl carbon of compounds **1**-**5**, which coincide well with the calculated results (19.11-22.3 ppm). Carbonyl carbons of *o*-benzoyl lactone and imino carbon [35] are appeared in the far downfield region at 161-154 ppm. In the present case, the characteristic signals appeared in the range of 163-159 ppm are assigned to *o*-benzoyl lactone and imino carbons.

3.8. Molecular electrostatic potential

The molecular electrostatic potential (MEP) mapping is a powerful tool that provides insights into reactive sites and physicochemical relationships as well as hydrogen-bonding interactions of a molecule [58].

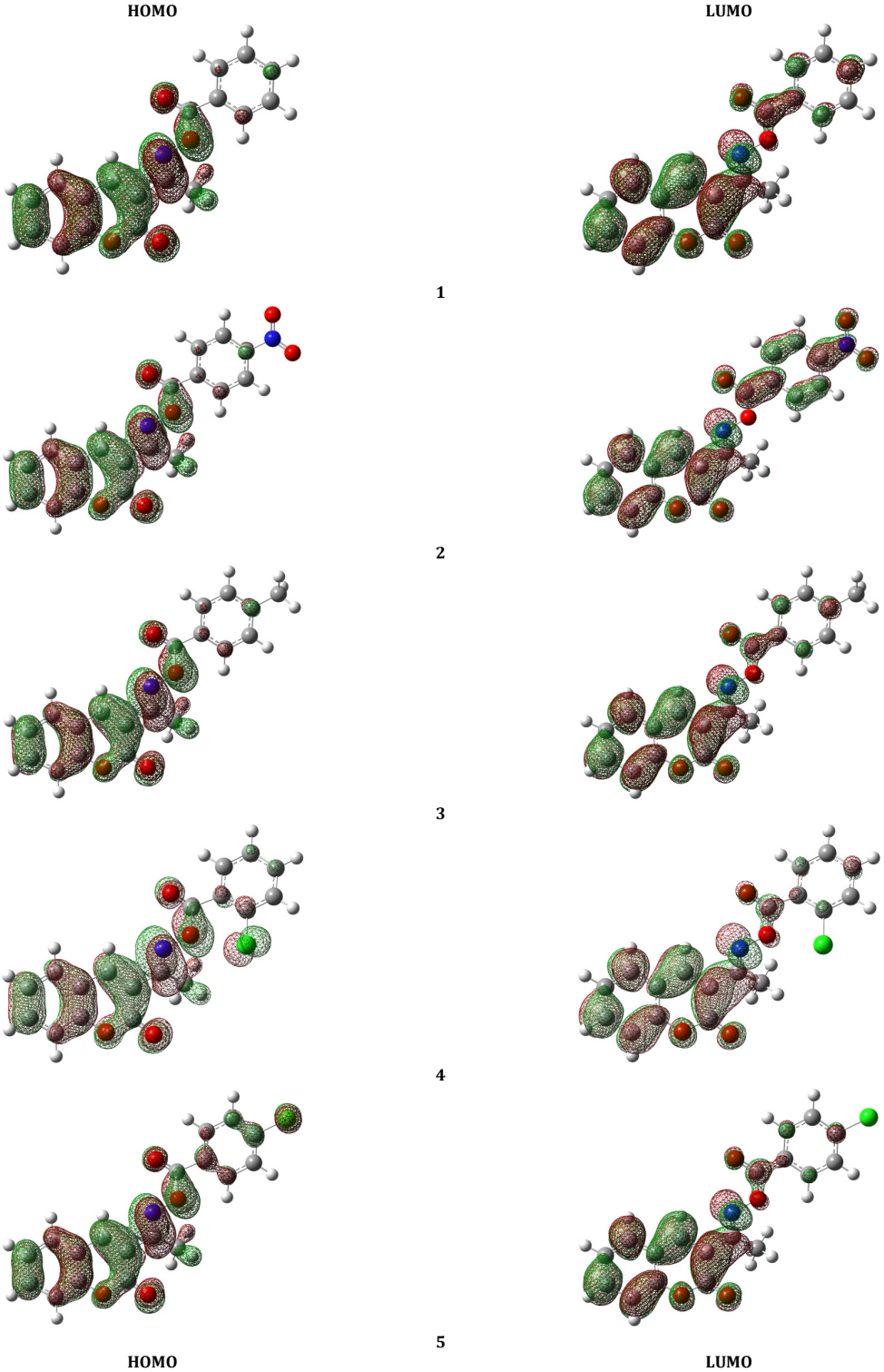

Figure 5. HOMO-LUMO plots of compounds **1-5**.

To predict the reactive sites of the synthesized molecules **1-5** MEPs are investigated. Figure 6 shows the electrostatic potential of compounds **1-5**, computed at 0.002 a.u. isosurface. The electrostatic potential increases in the order: red <orange < yellow < green < blue. The red (negative) regions of MEP were related to electrophilic reactivity and the blue (positive) regions to nucleophilic reactivity.

From the MEP pictures of compounds **1-5**, the electrophilic attacking site value determined by electron density from total SCF density mapped with total density to be -5.64, -5.49, -5.88, -5.76 and -5.74 kcal/mol and the nucleophilic attacking sites +5.64, +5.49, +5.88, +5.76 and +5.74 kcal/mol, respectively. The MEP values of compounds **1-5** reveal that the potential surface in favorable of electrophilic in nature. As seen in Figure 6, the oxygen atom of the pyrone ring (O11) and benzoyl (O18) segments carrying the red region which reveals the studied compounds are in favor of electrophilic attack. However, the light green region spread over the entire molecular surface, which indicates that the potential halfway between the two

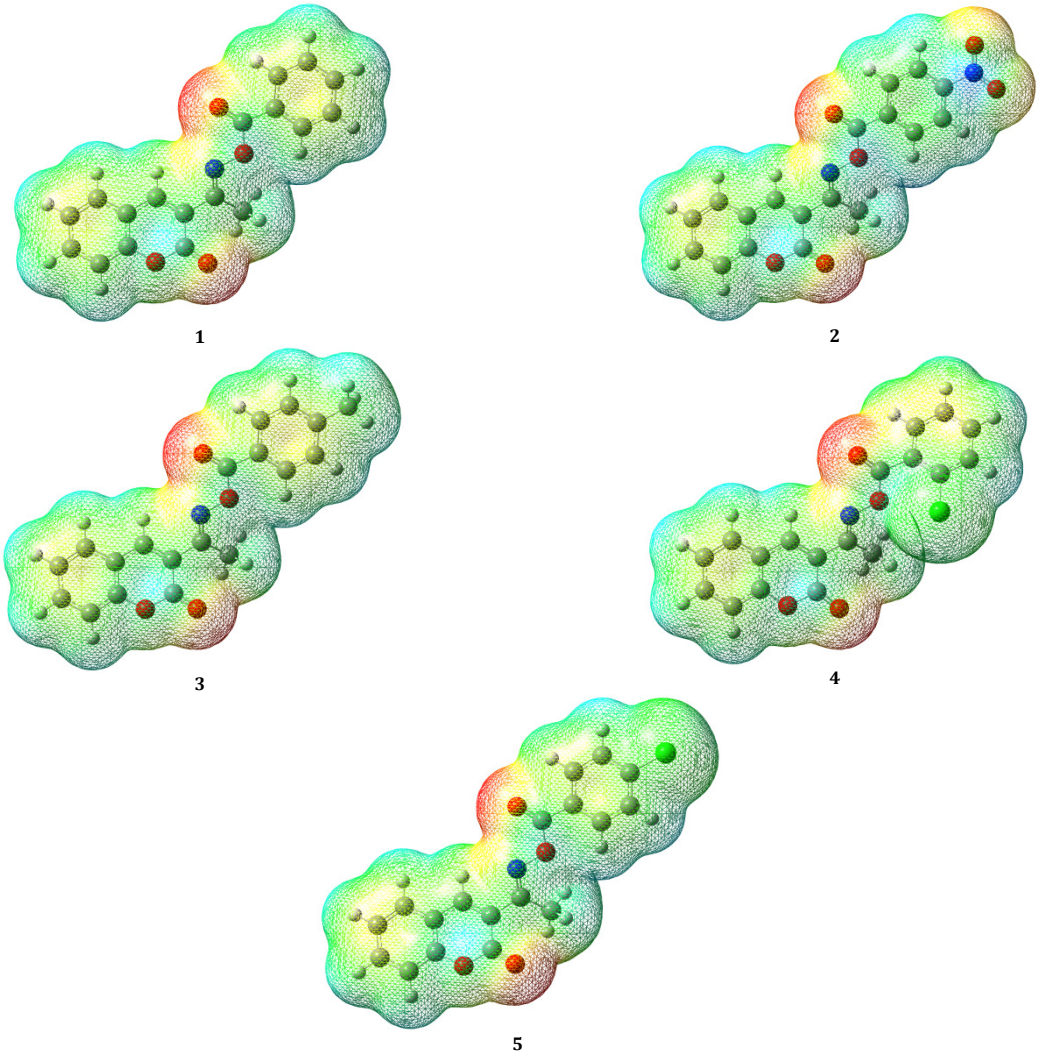

Figure 6. Molecular electrostatic potential model of compounds **1**-**5**.

extreme regions. From this MEP surface confirms the presence of an intermolecular interaction.

3.9. Non-linear optical properties

Non-linear optical (NLO) has one of the key functions in the field of photonic technology. It is a branch of optics that describes the interaction of a strong electromagnetic field with materials to create modified fields. A NLO material is one whose has high values of molecular polarizability and first-order hyperpolarizability [59]. For compounds **1**-**5**, the total dipole moment, molecular polarizability, and first-order hyperpolarizability have been calculated using B3LYP/6-311++G(d,p) method.

The total dipole moment (μ), mean polarizability (α), and mean first-order hyperpolarizability (β), using the *x*, *y*, *z* components are defined as

$$\mu = (\mu_x^2 + \mu_y^2 + \mu_z^2)^{1/2} \quad (2)$$

$$\alpha_0 = (\alpha_{xx} + \alpha_{yy} + \alpha_{zz})/3 \quad (3)$$

$$\alpha_{total} = 2^{-1/2}\left[(\alpha_{xx} - \alpha_{yy})^2 + (\alpha_{yy} - \alpha_{zz})^2 + (\alpha_{zz} - \alpha_{xx})^2 + 6(\alpha^2 xx + \alpha^2 yy + \alpha^2 zz)\right]^{1/2} \quad (4)$$

$$\beta_x = (\beta_{xxx} + \beta_{xyy} + \beta_{xzz}) \quad (5)$$

$$\beta_y = (\beta_{yyy} + \beta_{xxy} + \beta_{yzz}) \quad (6)$$

$$\beta_z = (\beta_{zzz} + \beta_{xxz} + \beta_{yyz}) \quad (7)$$

$$\beta_0 = (\beta_x^2 + \beta_y^2 + \beta_z^2)^{1/2} \quad (8)$$

The total dipole moment values computed using B3LYP/6-311++G(d,p) method are found to be decreased in the order: **2** > **5** > **4** > **1** > **3** and the trend of average polarizability are **2** > **5** > **4** > **3** > **1**, respectively. Besides, the average polarizability values of the synthesized compounds **1**-**5** are compared with *p*-nitroaniline. The results suggest that the studied compounds hold higher values than *p*-nitroaniline [60]. The computed hyperpolarizability value (β) of compounds **1**-**5** decreased in the order: **1** > **3** > **4** > **5** > **2**, respectively. Besides, the total first hyperpolarizability of compounds **2** (5.7478×10^{-30} esu) and **5** (2.073×10^{-30} esu) are superior to other compounds. Furthermore, the first hyperpolarizability values of compounds **1**-**5** are compared with urea (0.372×10^{-30} esu). The hyperpolarizability values (β) of compounds **2** and **5** are almost fifteen and six times superior to urea where as for other compounds, they are 1.6 and 2.2 times greater than urea [61]. In addition, the dipole moments of compounds **1**-**5** are higher than that of urea (1.373 Debye).

Table 6. Calculated thermodynamic parameters of compounds **1**-**5**.

Parameters	1	2	3	4	5
SCF energy (a.u.)	-1043.314	-1254.193	-1088.962	-1509.251	-1509.254
Total energy (kcal/mol)	181.340	184.306	199.558	175.997	176.020
Zero point energy (kcal/mol)	169.379	170.678	186.408	163.228	163.264
Rotational constants (GHz)					
x	0.586	0.554	0.572	0.474	0.574
y	0.126	0.076	0.105	0.114	0.084
z	0.110	0.072	0.094	0.105	0.078
Entropy (cal/mol.K)	148.358	162.726	158.471	154.337	155.490
Heat capacity (cal/mol.K)	73.451	82.204	79.544	77.374	77.364

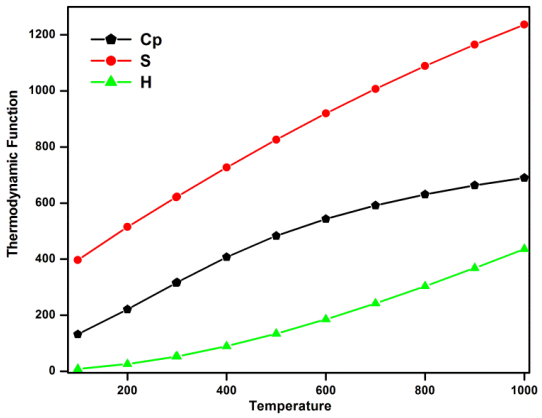

Figure 7. Correlation of the effect of temperature on heat capacity (Cp), entropy (S), and enthalpy change ($\Delta H_0 \rightarrow T$) of compound **1**.

From the above results, we conclude that the molecular polarizability and hyperpolarizability of the studied compounds **1**-**5** in all coordinates are active and so it can be used to prepare NLO crystals which may produce second order harmonic waves and among these the nitro derivative is the best NLO candidate for future study.

3.10. Thermodynamic properties

The temperature dependence of thermodynamic properties *viz*. the heat capacity, entropy, enthalpy change, and zero-point vibrational energy of compounds **1**-**5** have been calculated by B3LYP/6-311++G(d,p) technique and the values are summarized in Table 6. To bring the thermodynamic properties in accurately, the scale factors have been used [62,63]. The correlations of heat capacity, entropy, and enthalpy change with temperature for compound **1** are given in Figure 7. The obtained data shows that the entropy, heat capacity, and enthalpy changes increase with the increasing of temperature (100 to 1000 K). This is due to the molecular vibrational moments occurring and intensified at high temperature [64]. The calculated thermodynamic functions *vs* temperature with regression factor (R^2) are not less than 0.999 for all compounds **1**-**5**. The corresponding fitting equations for compounds **1**-**5** are

For compound **1**,
$Cp = 11.1043 + 1.1878T - 5.1105\times10^{-4}\ T^2$ $R^2 = 0.9994$
$S = 276.6924 + 1.2384T - 2.7869\times10^{-4}\ T^2$ $R^2 = 0.9999$
$\Delta H = -13.8385 + 0.1404T + 3.1437\times10^{-4}\ T^2$ $R^2 = 0.9994$

For compound **2**,
$Cp = 24.2911 + 1.2777T - 5.6447\times10^{-4}\ T^2$ $R^2 = 0.9995$
$S = 293.0813 + 1.4005T - 3.4369\times10^{-4}\ T^2$ $R^2 = 0.9999$
$\Delta H = -16.1186 + 0.1682T + 3.2895\times10^{-4}\ T^2$ $R^2 = 0.9994$

For compound **3**,
$Cp = 19.2660 + 1.2522T - 5.2999\times10^{-4}T^2$ $R^2 = 0.9994$
$S = 288.7109 + 1.3467T - 3.1110\times10^{-4}T^2$ $R^2 = 0.9999$
$\Delta H = -14.5778 + 0.1533T + 3.3627\times10^{-4}T^2$ $R^2 = 0.9995$

For compound **4**,
$Cp = 22.3297 + 1.2057 - 5.3285\times10^{-4}\ T^2$ $R^2 = 0.9996$
$S = 280.4842 + 1.3193 - 3.2353\times10^{-4}\ T^2$ $R^2 = 0.9999$
$\Delta H = -15.3265 + 0.1584 + 3.1004\times10^{-4}\ T^2$ $R^2 = 0.9994$

For compound **5**,
$Cp = 21.4665 + 1.2088 - 5.3522\times10^{-4}\ T^2$ $R^2 = 0.9996$
$S = 285.6887 + 1.318 - 3.2243\times10^{-4}\ T^2$ $R^2 = 0.9999$
$\Delta H = -15.3249 + 0.1582 + 3.1026\times10^{-4}\ T^2$ $R^2 = 0.9994$

It is seen from Table 6 that the trend of total energy and zero-point energy of the compounds **1**-**5**: **3** > **2** > **1** > **4** > **5**. The thermodynamic parameters like heat capacity, entropy, and enthalpy obtained at different temperatures are specified in decreased order: **2** > **3** > **5** > **4** > **1**. From Figure 7, it clearly reveals that the differences in entropy, heat capacity at constant pressure, and enthalpy change between compounds **1**-**3** are very small in magnitude and not significant.

4. Conclusion

Five substituted 3-(1-((benzoyloxy)imino)ethyl)-2*H*-chromen-2-ones (**1**-**5**) have been synthesized using 3-(1-(hydroxyimino)ethyl)-2*H*-chromen-2-one and substituted benzoic acids in presence of $POCl_3$ in pyridine. The calculated vibrational frequencies are matched well with the experimental results. The modes of vibrational assignment are allocated on the basis of PED calculations. The energy gap between HOMO and LUMO are in the trend of compounds **2** > **5** > **3** > **1** > **4**. Smaller, the energy gap of compound **2** reveals more reactive than the other compounds **1**, **3**-**5**. The NBO analysis reveals that the electron density of conjugated π-π* bonds of the benzoyl group and benzene ring of coumarin have clearly demonstrated strong delocalization. The calculated first hyperpolarizability value (β) of compound **2** is virtually fifteen times superior to the urea while the other compounds are in 6, 2.2, and 1.6. The thermodynamic parameters *viz*., entropy, heat capacity, and enthalpy changes are increased with increasing temperature from 100 to 1000 K. These increasing thermodynamic

parameters may be the molecular vibrational intensities increase with temperature.

Supporting information

CCDC-1036818 contains the supplementary crystallographic data for this paper. These data can be obtained free of charge via https://www.ccdc.cam.ac.uk/structures/, or by e-mailing data_request@ccdc.cam.ac.uk, or by contacting The Cambridge Crystallographic Data Centre, 12 Union Road, Cambridge CB2 1EZ, UK; fax: +44(0)1223-336033.

Disclosure statement

Conflict of interests: The authors declare that they have no conflict of interest.
Author contributions: All authors contributed equally to this work.
Ethical approval: All ethical guidelines have been adhered.
Sample availability: Samples of the compounds are available from the author.

ORCID

Kannan Gokula Krishnan
https://orcid.org/0000-0002-8223-557X
Venugopal Thanikachalam
https://orcid.org/0000-0002-2098-2641

References

[1]. Balandrin, M. F.; Klocke, J. A.; Wurtele, E. S.; Bollinger, W. H. *Science* **1985**, *228*, 1154–1160.
[2]. Murray, R. D. H.; Mendez, J.; Brown, S. A. *The Natural Coumarins: Occurance*; Chemistry and Biochemistry, Wiley: New York, 1982.
[3]. Sandhu, S.; Bansal, Y.; Silakari, O.; Bansal, G. *Bioorg. Med. Chem.* **2014**, *22*, 3806–3814.
[4]. Bhat, M. A.; Al-Omar, M. A.; Siddiqui, N. *Med. Chem. Res.* **2013**, *22*, 4455–4458.
[5]. Lacy, A.; O'Kennedy, R. *Curr. Pharm. Des.* **2004**, *10*, 3797–3811.
[6]. Arora, R. B.; Mathur, C. N. *Br. J. Pharmacol. Chemother.* **1963**, *20*, 29–35.
[7]. Singh, I. P.; Bharate, S. B.; Bhutani, K. K. *Curr. Sci.* **2005**, *89*, 269–290.
[8]. Leal, L. K.; Ferreira, A. A.; Bezerra, G. A.; Matos, F. J.; Viana, G. S. *J. Ethnopharmacol.* **2000**, *70*, 151–159.
[9]. Tyagi, Y. K.; Kumar, A.; Raj, H. G.; Vohra, P.; Gupta, G.; Kumari, R.; Kumar, P.; Gupta, R. K. *Eur. J. Med. Chem.* **2005**, *40*, 413–420.
[10]. Wang, Z.-S.; Hara, K.; Dan-oh, Y.; Kasada, C.; Shinpo, A.; Suga, S.; Arakawa, H.; Sugihara, H. *J. Phys. Chem. B* **2005**, *109*, 3907–3914.
[11]. Huang, Q.; Bao, C.; Ji, W.; Wang, Q.; Zhu, L. *J. Mater. Chem.* **2012**, *22*, 18275–18282.
[12]. Bazzicalupi, C.; Caltagirone, C.; Cao, Z.; Chen, Q.; Di Natale, C.; Garau, A.; Lippolis, V.; Lvova, L.; Liu, H.; Lundström, I.; Mostallino, M. C.; Nieddu, M.; Paolesse, R.; Prodi, L.; Sgarzi, M.; Zaccheroni, N. *Chemistry* **2013**, *19*, 14639–14653.
[13]. Rong, L.; Liu, L.-H.; Chen, S.; Cheng, H.; Chen, C.-S.; Li, Z.-Y.; Qin, S.-Y.; Zhang, X.-Z. *Chem. Commun. (Camb.)* **2014**, *50*, 667–669.
[14]. Secci, D.; Carradori, S.; Bolasco, A.; Chimenti, P.; Yáñez, M.; Ortuso, F.; Alcaro, S. *Eur. J. Med. Chem.* **2011**, *46*, 4846–4852.
[15]. Matos, M. J.; Vazquez-Rodriguez, S.; Uriarte, E.; Santana, L.; Viña, D. *Bioorg. Med. Chem. Lett.* **2011**, *21*, 4224–4227.
[16]. Politzer, P.; Murray, J. S. *The Chemistry of Hydroxylamines, Oximes and Hydroxamic Acids*; Wiley, West Sussex, 2009.
[17]. Krishnan, G., K.; Sivakumar, R.; Thanikachalam, V. *J. Serb. Chem. Soc.* **2015**, *80*, 1101–1111.
[18]. Karakurt, A.; Alagöz, M. A.; Sayoğlu, B.; Calış, U.; Dalkara, S. *Eur. J. Med. Chem.* **2012**, *57*, 275–282.
[19]. Bachovchin, D. A.; Wolfe, M. R.; Masuda, K.; Brown, S. J.; Spicer, T. P.; Fernandez-Vega, V.; Chase, P.; Hodder, P. S.; Rosen, H.; Cravatt, B. F. *Bioorg. Med. Chem. Lett.* **2010**, *20*, 2254–2258.
[20]. Sun, R.; Li, Y.; Lü, M.; Xiong, L.; Wang, Q. *Bioorg. Med. Chem. Lett.* **2010**, *20*, 4693–4699.
[21]. Liu, X.-H.; Pan, L.; Tan, C.-X.; Weng, J.-Q.; Wang, B.-L.; Li, Z.-M. *Pestic. Biochem. Physiol.* **2011**, *101*, 143–147.
[22]. Hwu, J. R.; Tsay, S.-C.; Hong, S. C.; Hsu, M.-H.; Liu, C.-F.; Chou, S.-S. P. *Bioconjug. Chem.* **2013**, *24*, 1778–1783.
[23]. Frisch, M. J.; Trucks G. W.; Schlegel, H. B.; Scuseria, G. E.; Robb, M. A.; Cheeseman, J. R.; Scalmani, G.; Barone, V.; Mennucci, B.; Petersson, G. A.; Nakatsuji, H.; Caricato, M.; Li, X.; Hratchian, H. P.; Izmaylov, A. F.; Bloino, J.; Zheng, G.; Sonnenberg, J. L.; Hada, M.; Ehara, M.; Toyota, K.; Fukuda, R.; Hasegawa, J.; Ishida, M.; Nakajima, T.; Honda, Y.; Kitao, O.; Nakai, H.; Vreven, T.; Montgomery, J. A.; Peralta, J. E.; Ogliaro, F.; Bearpark, M.; Heyd, J. J.; Brothers, E.; Kudin, K. N.; Staroverov, V. N.; Kobayashi, R.; Normand, J.; Raghavachari, K.; Rendell, A.; Burant, J. C.; Iyengar, S. S.; Tomasi, J.; Cossi, M.; Rega, N.; Millam, J. M.; Klene, M.; Knox, J. E.; Cross, J. B.; Bakken, V.; Adamo, C.; Jaramillo, J.; Gomperts, R.; Stratmann, R. E.; Yazyev, O.; A. J. Austin, A. J.; Cammi, R.; Pomelli, C.; Ochterski, J. W.; Martin, R. L.; Morokuma, K.; Zakrzewski, V. G; Voth, G. A.; Salvador, P.; Dannenberg, J. J.; Dapprich, S.; Daniels, A. D.; Farkas, O.; Foresman, J. B.; Ortiz, J. V.; Cioslowski, J.; Fox, D. J. Gaussian, Inc. , Gaussian 09, Revision A. 02, Wallingford CT, 2009.
[24]. Lee, C.; Yang, W.; Parr, R. G. *Phys. Rev. B Condens. Matter* **1988**, *37*, 785–789.
[25]. Becke, A. D. *J. Chem. Phys.* **1993**, *98*, 5648–5652.
[26]. Rauhut, G.; Pulay, P. *J. Phys. Chem.* **1995**, *99*, 3093–3100.
[27]. Scott, A. P.; Radom, L. *J. Phys. Chem.* **1996**, *100*, 16502–16513.
[28]. Wolinski, K.; Hinton, J. F.; Pulay, P. *J. Am. Chem. Soc.* **1990**, *112*, 8251–8260.
[29]. Krishnan, K.; Sivakumar, R.; Thanikachalam, V. *Lett. Org. Chem.* **2015**, *12*, 31–37.
[30]. Wang, H.; Xu, S.-H.; Zeng, Z.; Zhang, Y.-H. *Acta Crystallogr. Sect. E Struct. Rep. Online* **2010**, *66*, o511.
[31]. Vazquez-Rodriguez, S.; Uriarte, E.; Santana, L. *Acta Crystallogr. Sect. E Struct. Rep. Online* **2013**, *69*, o345.
[32]. Allen, F. H.; Kennard, O.; Watson, D. G.; Brammer, L.; Orpen, A. G.; Taylor, R. *J. Chem. Soc., Perkin Trans. 2* **1987**, S1-S19.
[33]. Silverstein, R. M.; Webster, F. X.; Kiemle, D. J. *The spectrometric identification of organic compounds: International edition*; 7th ed.; John Wiley & Sons: Nashville, TN, 2005.
[34]. Arjunan, V.; Sakiladevi, S.; Marchewka, M. K.; Mohan, S. *Spectrochim. Acta A Mol. Biomol. Spectrosc.* **2013**, *109*, 79–89.
[35]. Krishnan, K. G.; Sivakumar, R.; Thanikachalam, V.; Saleem, H.; Arockia doss, M. *Spectrochim. Acta A Mol. Biomol. Spectrosc.* **2015**, *144*, 29–42.
[36]. Arivazhagan, M.; Subhasini, V. P.; Kavitha, R. *Spectrochim. Acta A Mol. Biomol. Spectrosc.* **2014**, *128*, 527–539.
[37]. Palm, A.; Werbin, H. *Can. J. Chem.* **1953**, *31*, 1004–1008.
[38]. Stuart, B. H. *Infrared Spectroscopy: Fundamentals and Applications*; John Wiley and Sons: Chichester, UK, 2004.
[39]. Mariappan, G.; Sundaraganesan, N. *J. Mol. Struct.* **2014**, *1063*, 192–202.
[40]. Ayyappan, S.; Sundaraganesan, N.; Kurt, M.; Sertbakan, T. R.; Özduran, M. *J. Raman Spectrosc.* **2010**, *41*, 1379–1387.
[41]. Alcolea Palafox, M. *Int. J. Quantum Chem.* **2000**, *77*, 661–684.
[42]. Krishnan, K. G.; Kumar, C. U.; Lim, W.-M.; Mai, C.-W.; Thanikachalam, P. V.; Ramalingan, C. *J. Mol. Struct.* **2020**, *1199*, 127037.
[43]. Socrates, G. *Infrared and Raman characteristic group frequencies: Tables and charts*; 3rd ed.; John Wiley & Sons: Chichester, England, 2004.
[44]. Snyder, R. G.; Strauss, H. L.; Elliger, C. A. *J. Phys. Chem.* **1982**, *86*, 5145–5150.
[45]. Karuppasamy, A.; Gokula Krishnan, K.; Pillai Velayutham Pillai, M.; Ramalingan, C. *J. Mol. Struct.* **2017**, *1128*, 674–684.
[46]. Stalindurai, K.; Gokula Krishnan, K.; Nagarajan, E. R.; Ramalingan, C. *J. Mol. Struct.* **2017**, *1130*, 633–643.
[47]. Muthu, S.; Ramachandran, G.; Uma maheswari, J. *Spectrochim. Acta A Mol. Biomol. Spectrosc.* **2012**, *93*, 214–222.
[48]. Clarkson, J.; Smith, W. E.; Batchelder, D. N.; Smith, D. A.; Coats, A. M. *J. Mol. Struct.* **2003**, *648*, 203–214.
[49]. Mulliken, R. S. *J. Chem. Phys.* **1955**, *23*, 1841–1846.
[50]. Santamaria, R.; Cocho, G.; Corona, L.; González, E. *Chem. Phys.* **1998**, *227*, 317–329.
[51]. Reed, A. E.; Weinhold, F. *J. Chem. Phys.* **1985**, *83*, 1736–1740.
[52]. Snehalatha, M.; Ravikumar, C.; Hubert Joe, I.; Sekar, N.; Jayakumar, V. S. *Spectrochim. Acta A Mol. Biomol. Spectrosc.* **2009**, *72*, 654–662.
[53]. Cramer, C. J. Essentials of Computational Chemistry: Theories and Models, 2nd Ed., Wiley, Hoboken, NJ, 2004.
[54]. Udaya Sri, N.; Chaitanya, K.; Prasad, M. V. S.; Veeraiah, V.; Veeraiah, A. *Spectrochim. Acta A Mol. Biomol. Spectrosc.* **2012**, *97*, 728–736.
[55]. Sebastian, S.; Sylvestre, S.; Jayarajan, D.; Amalanathan, M.; Oudayakumar, K.; Gnanapoongothai, T.; Jayavarthanan, T. *Spectrochim. Acta A Mol. Biomol. Spectrosc.* **2013**, *101*, 370–381.
[56]. Basri, R.; Khalid, M.; Shafiq, Z.; Tahir, M. S.; Khan, M. U.; Tahir, M. N.; Naseer, M. M.; Braga, A. A. C. *ACS Omega* **2020**, *5*, 30176–30188.
[57]. Pavia, D. L.; Lampman, G. M.; Kriz, G. S.; Vyvyan, J. R. Introduction to Spectroscopy, 4th Ed., Brooks/Cole, Belmont, USA, 2009.
[58]. Scrocco, E.; Tomasi, J. Electronic molecular structure, reactivity and intermolecular forces: An euristic interpretation by means of electrostatic molecular potentials. In *Advances in Quantum Chemistry Volume 11*; Elsevier, 1978; pp. 115–193.
[59]. Nakano, M.; Shigemoto, I.; Yamada, S.; Yamaguchi, K. *J. Chem. Phys.* **1995**, *103*, 4175–4191.
[60]. Cheng, L. T.; Tam, W.; Stevenson, S. H.; Meredith, G. R.; Rikken, G.; Marder, S. R. *J. Phys. Chem.* **1991**, *95*, 10631–10643.
[61]. Wu, K.; Snijders, J. G.; Lin, C. *J. Phys. Chem. B* **2002**, *106*, 8954–8958.

[62]. Zhang, J.; Xiao, H. *J. Chem. Phys.* **2002**, *116*, 10674–10683.
[63]. Barone, V. *J. Chem. Phys.* **2004**, *120*, 3059–3065.
[64]. Rastogi, V. K.; Jain, V.; Yadav, R. A.; Singh, C.; Palafox, M. A. *J. Raman Spectrosc.* **2000**, *31*, 595–603.